Research Article | Vol. 10, No. 9 / 1 September 2020 / Optical Materials Express 2227
Optical Materials EXPRESS

Enhancement of the fluorescence property of carbon quantum dots based on laser ablated gold nanoparticles to evaluate pyrene

Amir Reza Sadrolhosseini,[1,*] Ganesan Krishnan,[2] Suhaidi Safie,[1,5,6] Mahnoush Beygisangchin,[1,3] Suraya Abdul Rashid,[3] and Sulaiman Wadi Harun[4]

[1]*Functional Device Laboratory, Institute of Advanced Technology, Universiti Putra Malaysia, 43400 UPM, Serdang, Selangor, Malaysia*
[2]*Laser Center, IBNU Sina Institute for Scientific and Industrial Research, Universiti Teknologi Malaysia, Johor Bahru, 81310, Malaysia*
[3]*Material Processing Laboratory, Institute of Advanced Technology, Universiti Putra Malaysia, 43400 UPM, Serdang, Selangor, Malaysia*
[4]*Department of Electrical Engineering, Faculty of Engineering, University of Malaya, 50603 Kuala, Lumpur, Malaysia*
[5]*co-corresponding author*
[6]*suhaidi@upm.edu.my*
[*]*amir17984818@gmail.com*

Abstract: Gold nanoparticles were prepared in a carbon quantum dots solution using the laser ablation technique to enhance the photoluminescence property of a carbon quantum dots solution. The gold plate was ablated using a Q-Switched Nd:YAG laser at 4, 8, 12, and 16 minutes with a stable laser energy. The optical properties, functional groups, and the morphology of the prepared samples were examined using UV-visible spectroscopy, Fourier transform spectroscopy, and transmission electron microscopy, respectively. When the ablation time increased, the size of the gold nanoparticles decreased from 20.69 nm to 13.52 and the plasmonic quality factor and concentration of the gold nanoparticles increased. The intensity peak of the photoluminescence carbon quantum dots solution increased in the presence of the gold nanoparticles and the interaction between the pure carbon quantum dots and the gold-nanoparticles/carbon quantum dots composite with pyrene were investigated using photoluminescence spectroscopy. Consequently, the variation in the photoluminescent peak in the presence of the gold nanoparticles was greater than the variation in the photoluminescence peak in the presence of pure carbon quantum dots. The detection limit was 1 ppm. Therefore, the gold nanoparticles not only enhanced the photoluminescence property of the CQD bath also it improved the interaction of the CQD with pyrene.

1. Introduction

Carbon quantum dots (CQD) are a class of nanostructure that are based on carbon material. They have promising properties that include high chemical stability, low toxicity, biofriendliness [1], and tuneable fluorescence emission [2,3]. CQD is a quasi-spherical carbon nanostructure with a particle size less than 10 nm [4]. The carbon atom also contains sp^2 bonding in the CQD [1,5]. The photoluminescence properties of CQD depend on the size of the particles and is due to a quantum confinement effect [6]. Hence, it is utilized for optoelectronic devices [5] and biotechnology applications, such as biosensors [3], bioimage [7], and a photocatalyst [8,9]. CQD has an adjustable fluorescence property duo for size and excitation, so it produces photoluminescence emission in the long-wavelength (red or NIR region) [2]. Hence, CQD can

#396914 https://doi.org/10.1364/OME.396914
Journal © 2020 Received 4 May 2020; revised 28 Jun 2020; accepted 28 Jun 2020; published 24 Aug 2020
Corrected: 23 Sep 2020

Optical Materials EXPRESS

be used for drug delivery [10] since the background shining from the internal fluorophores can be avoided during the imaging process [2].

Three main mechanisms can be used to explain fluorescence emission from CQD. The first originates from conjugated π-domains [1]; the second is based on surface defects and the surface state [11,12], the third model depends on the molecular state [11,12]. On the other hand, the photons that are emitted from the electronic transition of the CQD core are influenced by the quantum confinement effects [13]. Hence, the photon energy depends on the particle size [14] of CQD. CQD has an adjustable fluorescence property based on the quantum confinement effect used in chemical sensors [2]. One of the more interesting application of CQD is as a chemical sensor, i.e. sensing copper [15], lead [16], chromium [17], and mercury [18]. Indeed Goncalves et al. used the CQD to detect the Hg ion and they achieved efficient quenching in the photoluminescence intensity of CQD in the presence of micromole concentration of the Hg ion. Consequently, CQD has a potential for use as a chemical sensor.

Gold nanoparticles (Au-NPs) have attractive plasmonic properties [19] and thus have applications in both medical and industrial researches. Au-NPs can be found in different shapes, including nanorods, nanowires, nanotubes, spherical nanoparticle and nanoplates [19]. Anisotropic gold nanoparticles including spherical Au-NPs, are the source of plasmonic [20] properties in the visible range. The plasmonic properties of Au-NPs are due to a surface plasmon resonance (SPR) of free electron oscillation that occurs on the surface of the gold nanoparticles [21]. SPR occurs in the UV-visible range and causes optical absorption and scattering of a visible photon with Au-NPs [22,23]. Thus, Au-NPs can be used for photothermal therapy [24], biochemical, biological sensors [25] and optoelectronic devices [26]. Therefore, gold nanoparticles are one of the most popular nanoparticles used for the enhancement of the plasmonic properties of nanocomposite, such as fluorescence and Raman properties.

Gold nanoparticle can be prepared in an aqueous solution using the chemical method, the biological [27,28] method and certain physical methods such as the seeded-growth method [29], the microorganism method [29], the microwave method [30], the sonochemical method [31], the gamma radiation [32] technique and the laser ablation technique.

Recently, researchers used the Au-NPs to improve and enhance the surface properties [33], plasmonic, and fluorescence properties of carbon quantum dots [34]. The Au-NPs/CQD composite has the potential to detect heavy metal [35], pesticides [36], glucose [37], iodine ion in an aqueous solution [38] and thiol drugs [39]. Indeed, Au-NPs/CQD has a high potential of interacting with many toxic chemicals.

Gold nanoparticles/carbon quantum dot composite were prepared using the hydrothermal methods [40], a chemical method and the physical mixture method [41] for biological application [39], detection of pesticides [36], and cyanide ions (CN^-) the aqueous solutions [41]. The applications are based on the enhancement fluorescence properties of CQD. The preparation methods carried out key steps and used the chemical agents needed.

The laser ablation method is a simple, fast, and green method used to prepare high-purity gold nanoparticles in a liquid solution. These gold nanoparticles generate in the liquid solution from the vaporization of gold plate [42] and gold nanoparticles form in the liquid solution without any chemical agent [42]. The laser energy is in the range of 650 to 1000 mJ [42] and the purity of the final product depends on the purity of the gold plate and the liquid solution. Laser ablation was used to prepare the gold nanoparticles [43] in both organic and inorganic solvents.

Laser ablation is one of the physical methods used to prepare CQD [44,45]. The particle size was in the range of 1.5 to 10 nm [44–46] and the laser energy was about 12.5 J/cm^2 [45]. Laser ablated CQD was used for light emission [45] photoluminescence emission from biomass for cellular imaging [44], and biomedical and therapeutic applications [46,47]. The absorption peak of CQD falls in the violet [1] range, and the wavelength of the laser for preparation of nanoparticles is usually in the green or near-infrared range of the UV-Vis spectrum. Hence, laser

Optical Materials EXPRESS

ablation can be used for preparing nanoparticles in the CQD solution. In addition, the laser energy for preparing CQD is more than the energy necessary for preparing of metal nanoparticles, such as gold nanoparticles.

In this study, carbon quantum dots were prepared using the acid-free hydrothermal method and an empty fruit bunch biochar. The prepared sample was used to synthesis the gold nanoparticles/carbon quantum dots composite solution using the laser ablation method. The main goal is enhancement and improvement of the photoluminescence property of CQD and the interaction of CQD with pyrene as a toxic chemical. The prepared Au-NPs/CQD composites were characterized using a UV-Visible spectroscopy. Fourier transform infrared spectroscopy and transmission electron microscopy. The fluorescence property of Au-NPs/CQD was investigated using photoluminescence spectroscopy, which used to recognize the low concentration of the pyrene.

2. Methodology

2.1. Preparation of carbon quantum dots (CQD)

The preparation of CQD was reported in Ref. [39]. Empty fruit bunch biochar was used for the preparation of carbon quantum dots in acid-free medium. The empty fruit bunch biochar was derived from the carbon source using isopropanol as a co-solvent. The water/isopropanol ratio was 3:1. Just as in a typical process, 0.06 g of EFB biochar was added into a cylindrical steel tube. Then, 6 mL of the co-solvent mixture was added into the same tube. It was then sonicated for 5 minutes before being put into an oven at temperature 250°C for 60 minutes. Upon completion of the heating process, the cylindrical steel tube was left immersed in a water bath to cool down for about 4 hours. The black liquid produced was purified using centrifugation (4000 rpm, 5 minutes) to eliminate the residual biochar [48]. The supernatant containing CQD was withdrawn and kept for further characterization.

To prepare the Au-NPs, the compounds of gold element should be used in an acidic or an alkaline medium but the CQD was prepared using the acid-free hydrothermal. Hence, the prepared CQD was used to prepare the Au-NPs using the laser ablation technique.

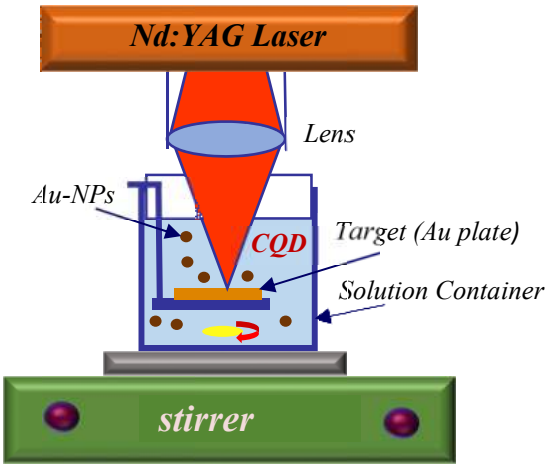

Fig. 1. The laser ablation setup contains a Q-switch Nd:YAG laser (1064 nm), lens, target (Au plate), solution container, and stirrer.

Optical Materials EXPRESS

2.2. Laser ablation methods

Figure 1 shows the laser ablation set up [49] for the preparation of Au-NPs in CQD solution, which involved the use of Q-switch Nd:YAG laser at 1064 nm wavelength. The laser beam in the 800 mJ and 40 Hz repetition rate frequency was ablated a high purity Au metal plate (99% Sigma Aldrich) which was immersed in 50 ppm concentration of CQD solution. The ablation time was 4, 8, 12 and 16 minutes. The prepared samples were characterized in the solution form using UV-visible spectroscopy (UV-vis) and Fourier transform infrared spectroscopy (FT-IR). The shape of nanoparticles was investigated using transmission electron microscopy (TEM).

3. Results and discussion

FT-IR experiments were carried out for the investigation of functional groups in CQD and Au-NPs/CQD solutions. Figures 2(a) and 2(b) show the FT-IR spectra of the pure CQD and Au-NPs/CQD solutions. The main peaks appeared at 3265.66, 3266.73, 2168.14, 2128.36, 1630.03, 1635, 1410.1, 1432.87, 1100.32,1132.02, and 448.66 cm^{-1}. The peaks at 3265.66 and 3266.73 cm^{-1}related to O-H and the peaks at 1630.03 and 1635 cm^{-1} assigned the C = O stretching vibration at the edge of the CQD molecule. The broad peaks at 2168.14 and 2128.36 cm^{-1} corresponded with C≡C bond's weak [50] stretching and the peaks at 1410.1 and 1432.87 cm^{-1} represented the C = C, O-H stretching vibration at the surface and the edge of CQD. The peaks at 1100.32 and 1132.02 cm^{-1} corresponded to C-O stretching vibration in the CQD. The peak at 448.66 cm^{-1} occurred in the fingerprint area, and it is related to the Au-NPs. The peaks related to C-O and C = C stretching vibration shifted to 1432.97 and 1132.02 cm^{-1}, respectively. Indeed, the shift of peak from 1100.32 cm^{-1} to 1132.02 cm^{-1} is due to capping the Au-NPs with CQD using C-O at the edge of CQD molecule. In addition, the peak at 1410.1 cm^{-1} shifted to 1432.87 cm^{-1} [51] that corresponded to interaction of Au-NPs with hydroxyl group at the edge of CQD [51]. Moreover, the intensity of peak at 1630 cm^{-1} decreased and the peak at 2168.14 cm^{-1} shifted to 2128.36 cm^{-1} and the intensity of peak increased. Consequently, the Au-NPs formed in the CQD solution and CQD capped the Au-NPs [52].

Figures 3(a), 3(b), 3(c), and 3(d) show the UV-vis spectra of the Au-NPs/CQD composite solution for the different ablation times ranging from 4 min to 16 min. The main peaks appeared at 368, 523, 520, 514, and 510 nm. The peak at 368 nm related to functional groups containing O at the edge of CQD and depended on the n-π* transition of oxygen at the edge of the carbon quantum dots structure [53,54]. Other peaks that occurred at 523, 520, 514, and 510 nm, arose from the localized surface plasmon resonance of Au-NPs. The UV-vis peaks showed a blue shift, which can be explained using Mie's theory [55]. The UV-Vis peaks for Au-NPs arose from the localized surface plasmon resonance. It depends on particle size and is due to long-range dipole coupling occurring in the Au-NPs [56]. In addition, the light beam excites the localized surface plasmons wave at the interface of Au-NPs and CQD. In accordance with Mie's theory the absorption cross section ($\sigma_{abs} \propto d^3/\lambda$) [57–59] of Au-NPs in the spherical shape is proportional to particle size(d) and reverse of wavelength (λ). Therefore, when the particle size decreased ($\lambda \propto d^3/\sigma_{abs}$), the blue shift occurred, and the scattering cross-section increased. Consequently, the particle size decreased as the ablation time increased.

Figure 3(e) depicts the experimental results for the transmissivity and the reflectivity spectra of Au-NPs/CQD solutions. These experiments were carried out from 300 nm to 600 nm. The spectra were analysed using Beer's Lambert law to obtain information about the dielectric constant of the samples. It was also used to evaluate the plasmonic quality of the Au-NPs/CQD composite. The relationship between the absorbance and transmissivity (T) of the Au-NPs/CQD composite was as follows [51]:

$$\begin{aligned} absorbance &= -\log_{10} T \\ T &= I/I_0 \end{aligned} \tag{1}$$

Optical Materials EXPRESS

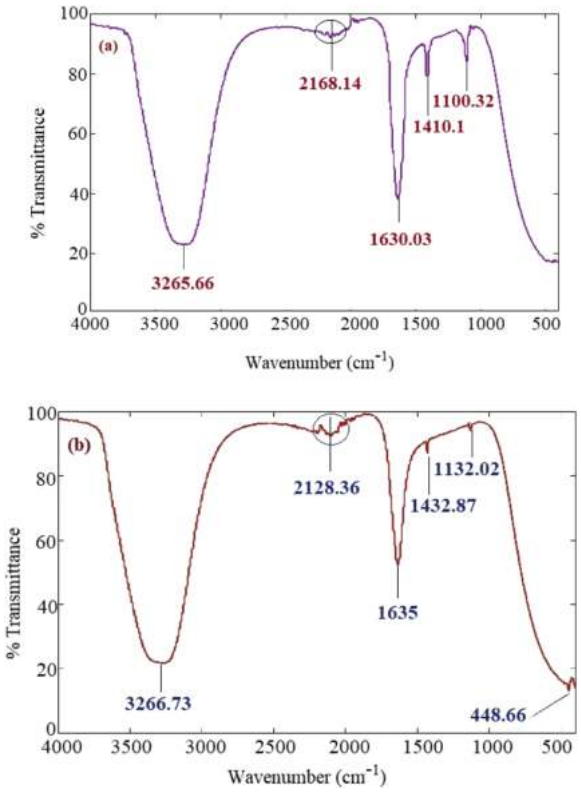

Fig. 2. The FT-IR spectrum for a) pure CQD and b) Au-NPs/ CQD solution in 16 min ablation time.

where I_0 and I are the intensity of the incident light beam and the transmitted beam, respectively. The optical density (OD) and the absorbance are equal, and proportional to the absorption coefficient of the Au-NPs/CQD composite solution as follows:

$$OD = 0.434 \times \alpha \times l \tag{2}$$

where l is the optical path (l) and it is 1 cm in this experiment. Reflectivity (R) is a function of the refractive index and can be expressed as follows:

$$R = ((n-1)^2 + k^2)/((n+1)^2 + k^2) \tag{3}$$

The dielectric constant is expressed as follows:

$$\varepsilon = \varepsilon_r + i\varepsilon_i \tag{4}$$

where ε_r and ε_i are the real and imaginary parts of the dielectric constant. The relationship between the real and imaginary parts of the dielectric constant with the refractive index of the solution is as follows:

$$\varepsilon_r = n^2 - k^2 \tag{5}$$

$$\varepsilon_i = 2nk \tag{6}$$

Consequently, the value of the dielectric constant can be calculated from the UV-visible spectrum using Eqs. (2), (3), (5) and (6). The reflectivity and transmissivity of the spectra in Fig. 3(b)

Optical Materials EXPRESS

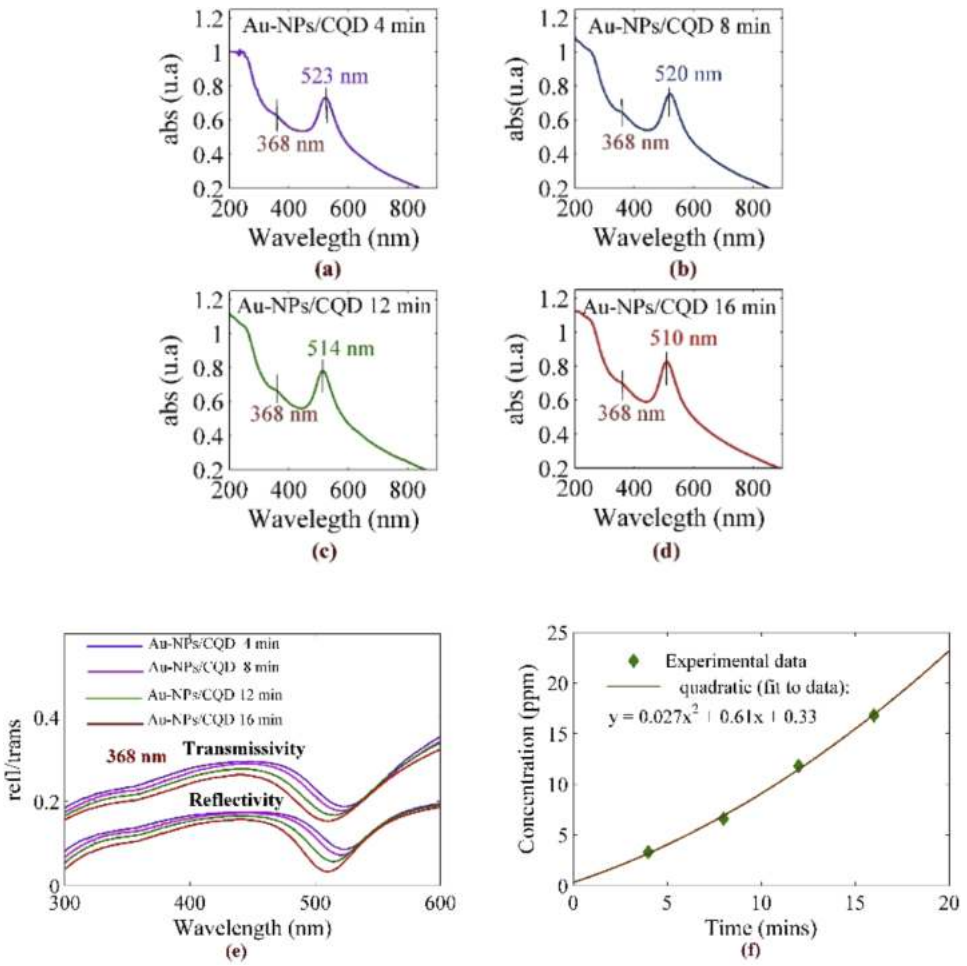

Fig. 3. Absorption spectrum for Au-NPs/CQD composite in the a) 4 min, b) 8 min, c)12 min, d) 16 min ablation time. e) Transmissivity and reflectivity spectrum for Au-NPs/CQD composite. f) variation for the concentration of Au-NPs inside the CQD with ablation time

Table 1. Optical parameters for Au-NPs/CQD composite solution

Sample	ε_r	ε_i ($\times 10^{-7}$)	α	Qf ($\times 10^6$)
Au-NPs/CQD 4 min	3.203	2.528	1.697	-12.7
Au-NPs/CQD 8 min	2.973	2.479	1.734	-11.9
Au-NPs/CQD 12 min	2.662	2.381	1.784	-11.7
Au-NPs/CQD 16 min	2.158	2.217	1.863	-9.8

Optical Materials EXPRESS

were analysed using the Fresnel theory, and the dielectric constant and absorption coefficient for Au-NPs/CQD composite solutions at absorption peaks were also calculated. The results are presented in Table 1.

The absorption peaks in UV-vis arose from localized surface plasmon resonance and the optical absorption or extinction was maximum at the localized surface plasmon resonance frequency. Moreover, the absorption cross-section at a localized surface plasmon resonance frequency was more effective than the absorption cross-section in the other parts, and further, the plasmonic quality factor depends on the dielectric constant of the solution as follows [41,60,61]:

$$Qf = -\frac{\varepsilon_r}{\varepsilon_i} \tag{7}$$

where ε_r and ε_i are the real and imaginary parts of the Au-NPs/CQD composite solution at the absorption peaks including 510, 514, 520, and 523 nm . As a result (see Table 1), the plasmonic quality factor at the absorption peak for Au-NPs/CQD composite is in the range of -12.7×10^6 to -9.8×10^6. The concentration of Au-NPs was measured using atomic absorption spectroscopy (AAS) and was in the range of 3.3 ppm to 16.8 ppm. Figure 3(f) shows that the concentration of Au-NPs increased when the ablation time increased from 4 to 16 mins because the interaction time for the laser beam with the target and the number of nanoparticles that released to the CQD solution increased. This process caused an increase in the concentration of Au-NPs. When the ablation time increased, the absorption coefficient of the solution also increased, and caused the increase in the plasmonic quality factor. On the other hand, the imaginary part of the dielectric constant was proportional to the concentration of Au-NPs. Therefore, the plasmonic quality factor increased.

Figures 4(a) and 4(b) show the TEM images of pure CQD. Figure 4(a) shows the distribution of CQD in the solution at a particle size of about 3.5 nm. Figure 4(b) shows the high magnification TEM of CQD where the dots depict good crystallinity with lattice fringes of about 0.21 nm, which thereby relates to the (100) plane of graphitic carbon [62].

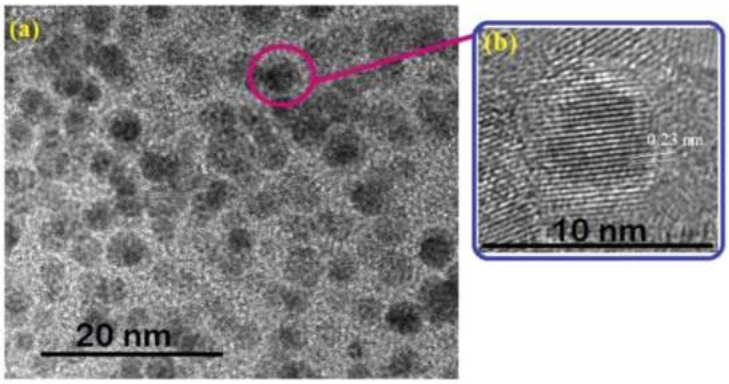

Fig. 4. a) The TEM image of pure CQD. b) High magnification of small part of a) that was depicted with pink cycle and it show lattice of CQD.

Figure 5 shows the TEM images and the analysis of the image carried out using Image J software to obtain the particle size. As a result, spherical- shaped Au-NPs formed in the CQD solution. The particle size was from 20.69 nm to 13.52 nm. The particle size decreased as the ablation time increased, so the TEM image confirmed the blue shift in the UV-vis spectrum. Figures 5(a3), 5(a4), 5(b3), 5(b4), 5(c3), 5(c4), 5(d3), and 5(d4) show the images of an Au-NPs and CQD contact together. The image of the yellow circle area is presented in a higher magnification than Figs. 5(a1), 5(b1), 5(c1), and 5(d1) which show that the CQD attached to Au-NPs. The particle

Optical Materials EXPRESS

size and the concentration of particles both depend on the energy of the laser beam in the laser ablation technique. Hence, the results are repeatable given the same conditions.

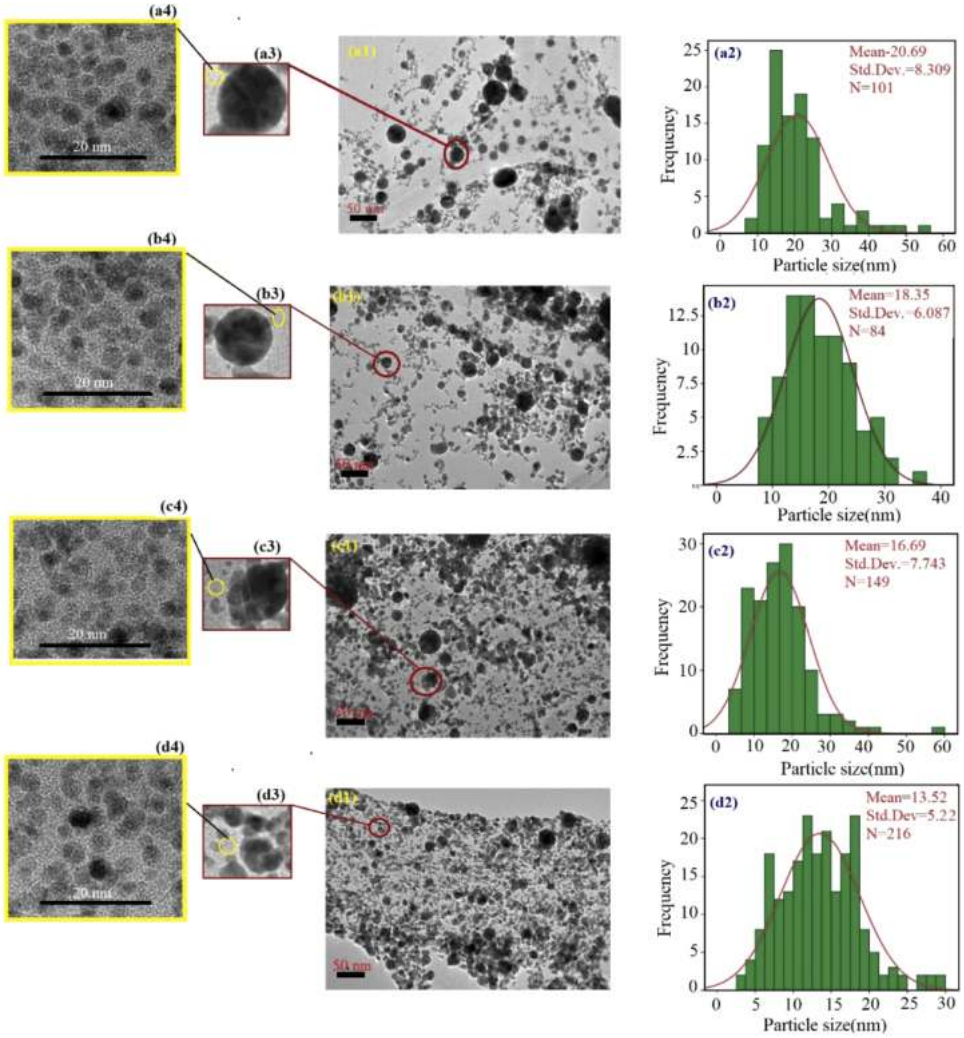

Fig. 5. TEM image for Au-NPs/CQD composite solution a) 4 min, b) 8 min, c)12 min, and d)16 min

Figure 6(a) shows excitation spectra exciting the photoluminescence of the pure CQD and Au-NPs/CQD. The excitation peaks occurred at 256 nm. When the sample was excited with light beam, the photons of the light beam were absorbed by Au-NPs/CQD. Hence, the intensity peaks increased in the excitation spectra. Figure 6(b) shows the emission spectra that are related to photoluminescence emit for the pure CQD and Au-NPs/CQD solutions for different ablation times. The samples were excited at 256 nm, and emission occurred at 336 nm. The intensity of the photoluminescence increased as the concentration of Au-NPs increased. The volume fraction of the nanoparticles for Au–NPs/CQD 16 mins ablation time was greater than the volume fraction of nanoparticles for Au-NPs/CQD 2 mins ablation time. Thus, the light scattering and the cross-section for the scattering of the light beam increases as an increase also occurs for the ablation time and concentration of Au-NPs in CQD solutions. Figure 6(b) shows the variation in photoluminescence intensity for Au-NPs/CQD for the different concentrations at an emission

Optical Materials EXPRESS

peak and that the variation of intensity peak is in quadric form. The photoluminescence emission of Au-NPs/CQD is related to the functional group on the CQD and the Au-NPs provides the free electron and increases the cross-section. Therefore, the photoluminescence emission intensity is enhanced. Moreover, the excitation peaks correspond to absorb the photon with an Au-NPs/CQD composite. while the intensity of the excitation peak increased as the concentration of Au-NPs in the composite also increased.

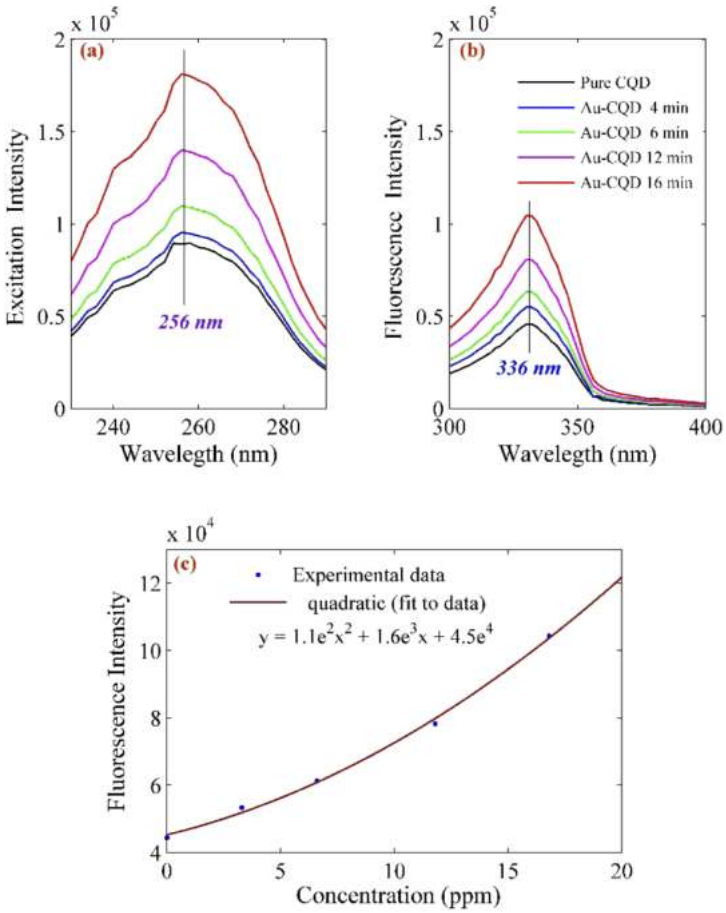

Fig. 6. a) The excitation spectra to excite the Photoluminescence of pure CQD and Au-NPs/CQD solutions in the different ablation time. b) The emission spectra related to excite the photoluminescence of pure CQD and Au-NPs/CQD composite solution in the different ablation time. c) Variation of photoluminescence intensity at the emission peak.

The photoluminescence properties of CQD depend on the size. Two approaches can be used to explain the photoluminescence mechanism. The surface state and the confinement effect represent the excitation-dependent [63–65] photoluminescence in CQD. The surface defect and the degree of carbonization are exhibited in the excitation-independent [66] photoluminescence emission.

The first and second approaches are related to bandgap transitions by the domains and surface defects on the surface of the CQD molecular [67]. Hence, the first approach has very strong absorption and weak emission, whereas the second approach has weak absorption and strong emission [68]. Figure 6(a) shows the excitation at 256 nm and the strong emission at 332 nm. The photoluminescence intensity of Au-NPs/CQD is stronger than pure CQD because the Au-NPs

Optical Materials EXPRESS

have free electron that can be transferred between the Au-NPs and carbon, and the popularity of the electron increased. Thus, the Au-NPs can donate the electron to CQD, which causes the change in the electronic specification of CQD. Consequently, the fluorescence is enhanced [69]. The plasmonic quality factor of Au-NPs/CQD increases as the ablation time increases which means that an increase occurred in the effectiveness of the cross-section, thereby producing an enhancement of the photoluminescence property.

As a result, the Au-NPs/CQD solution in just 16 mins has the highest plasmonic quality factor. This sample was thus chosen to investigate the detection of the pyrene. Figure 7(a) depicts the photoluminescence spectra for an evaluation of the different concentrations of pyrene (1,2,5,10 and 15 ppm) using Au-NPs/CQD in 16 mins ablation time. As a mentioned above the absorption cross-section depends on the *Qf,* which is the reason for the enhancement of the photoluminescence, which than is enhanced by the free electron from Au-NPs that interacted with CQD. The Au-NPs/CQD was contacted to pyrene with the different concentrations. Figure 7(a) shows the excitation intensity that excites the photoluminescence when the Au-NPs/CQD is contacted with pyrene, and the peaks appeared at 256 nm. Figure 7(b) depicts the photoluminescence emission related to the Au-NPs/CQD composite and the peaks that occurred at 336nm. As a result, the emission peaks decreased when the concentration of pyrene increased from 1 ppm to 15 ppm. Figure 7(c) shows the excitation intensity when the pure CQD interacted with different concentration of pyrene. Further, the emission peaks appeared at 336 nm, and this peak was used to compare the results when the Au-NPs/CQD adsorbed the pyrene. In accordance with Fig. 6(a), the excitation peak for CQD was at 256 nm, and the emission peaks also appeared at 336 nm [Fig. 6(b)]. As a result [Fig. 7(d)], the intensity peak of photoluminescence decreased at the peak of emission when the concentration of pyrene increased from 1 to 15 ppm in the presence of pure CQD. The variation in peak intensity is shown in Fig. 7(e) (red curve). Consequently, the slope of the variation curve (red curve) is about 50.88°. The experiment was continued with pure CQD. Figures 7(c) and 7(d) showed excitation and photoluminescence emission when the pure CQD was interacted with the different concentrations of pyrene. The emission peaks also showed that when the concentration of pyrene increased, the intensity of the photoluminescence peak decreased while the variation of the intensity peak with a concentration of pyrene was demonstrated in Fig. 7(e) (green curve). The slope of the variation curve (green curve) was about 21.15°.

The main activities in this study were the investigation of optical properties and the application of an Au-NPs/CQD composite. To evaluate the advantage of Au-NPs/CQD over pure CQD, the variation of the intensity peak was compared for both cases. The slope of the variation curve (red curve) when Au-NPs/CQD interacted with pyrene was greater than the slope of the variation curve when pure CQD interacts with pyrene. Therefore, the sensitivity of Au-NPs/CQD to the detection of pyrene is higher than that for pure CQD, and Au-NPs improved the fluorescence property of CQD.

The photoluminescence test carried out repeatedly 10 times to evaluate the stability of the photoluminescence properties of the Au-NPs/CQD solution. The average intensity of photoluminescence and the standard deviation were 10.40×10^4 and 0.1422×10^3, respectively.

The photoluminescence test carried out 10 times to evaluat the stability of the photoluminescence properties of Au-NPs/CQD solution. The average intensity of photoluminescence and the standard deviation (σ) were 10.40×10^4 and 0.1422×10^3, respectively. The limit of detection (LOD) is proportinal to standard deviation (σ) and slop (K) of variation of photoluminescence intensity with concentration of pyrene. Therefore, the LOD ($LOD = (3\times\sigma)/K$) was achieved about 8.38.

Figure 8(a) shows the interaction between CQD and Au-NPs derived from the FT-IR spectrum. As a result, the CQD can strongly cap the Au-NPs with hydroxyl and carboxyl groups at the edge of the CQD molecule. Au-NPs have high plasmonic property, so they can donate their

Optical Materials EXPRESS

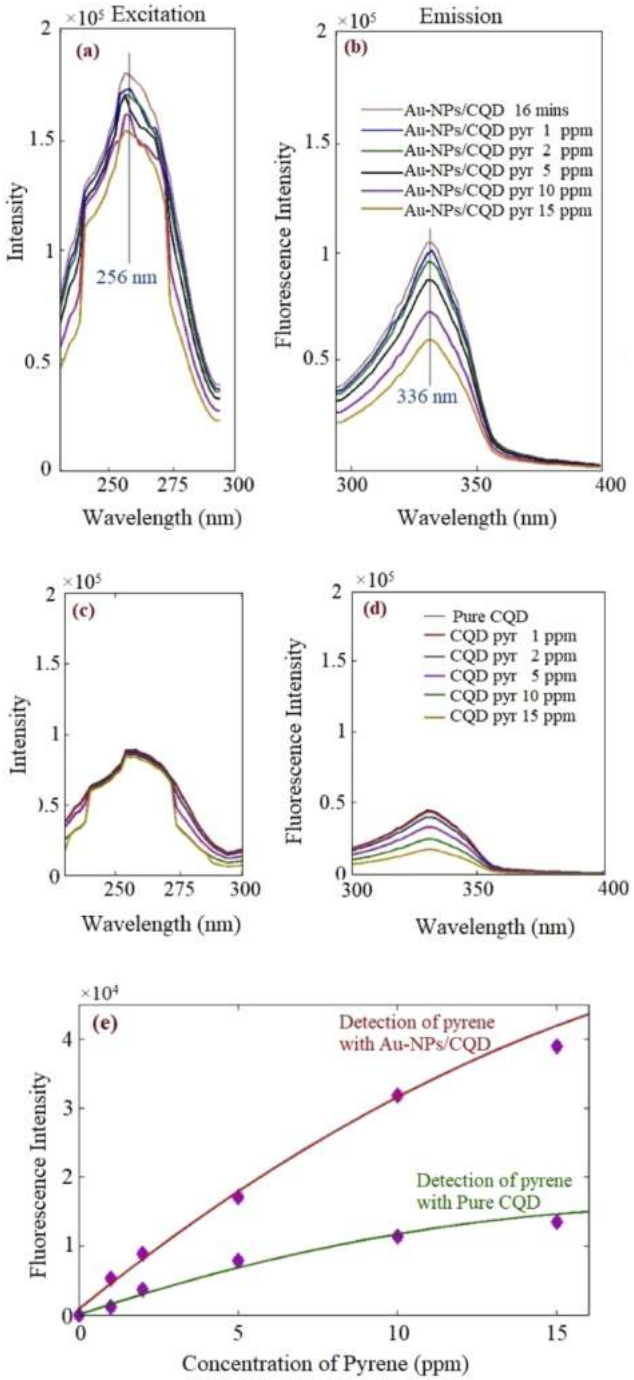

Fig. 7. a) The peaks at 265 nm are the residual radiation from the excitation source. b) The peaks at 336 nm are the emission photoluminescence for a detection of pyrene in a concentration of 1 ppm, 2 ppm, 5 ppm, 10 ppm, and 15 ppm when the Au-NPs/CQD interacted with pyrene. c) The excitation peak. d) A photoluminescence emission for the detection of pyrene using pure CQD when the concentration of pyrene is in the range of 1 ppm to 15 ppm. e) Variation of intensity peaks when the Au-NPs/CQD (red line) and the pure CQD (green line) interacted with pyrene.

Optical Materials EXPRESS

free electron to the CQD molecule. Therefore, the main mechanism of photoluminescence and the detection of pyrene could explain based on the photoluminescence property of CQD and Au-NPs/CQD which corresponds to the surface -related defective sites which generally refers to any sites that have nonperfect sp^2 domains that will result in surface energy traps. Both sp^2 and sp^3 hybridized carbons, and also the carbonyl group as a localized electronic state, contribute to the CQD and Au-NPs/CQD [see Fig. 8(b)] emissions in the blue range. Thus a mechanism is like the aromatic molecules are individually incorporated into solid hosts, thereby exhibiting CQD and Au-NPs/CQD emissions due to the existence of multiple surface defects with different excitation and emission properties [67,68]. As a result, the excitation of the molecule was 256 nm and the emissions were 336 nm while Au-NPs enhanced the intensity of the photoluminescence spectrum. The emissions occurred from CQD and Au-NPs provided the extra electron that contributed to enhancing the photoluminescence and intensity with pyrene. So, the Au-NPs enhanced the photoluminescence property of CQD. Here, Au-NPs served as a donator of an electron to CQD. Moreover, Au-NPs can interact with pyrene and is the interface between CQD and pyrene. The photoluminescence intensity depends on the population of the electron that transfers during the electronic state of CQD, and when the concentration of pyrene increased, the population of the electron that shared between Au-NPs and CQD decreased. Therefore, the intensity of the photoluminescence decreased when the population of free electron decreased, and the optical parameters such as the absorption coefficient (α) and the imaginary part of the refractive index ($k = \alpha \times \lambda/4\pi$) changed. Consequently, Au-NPs can enhance the photoluminescence of CQD and are sensitive enough to interact with a low concentration of pyrene.

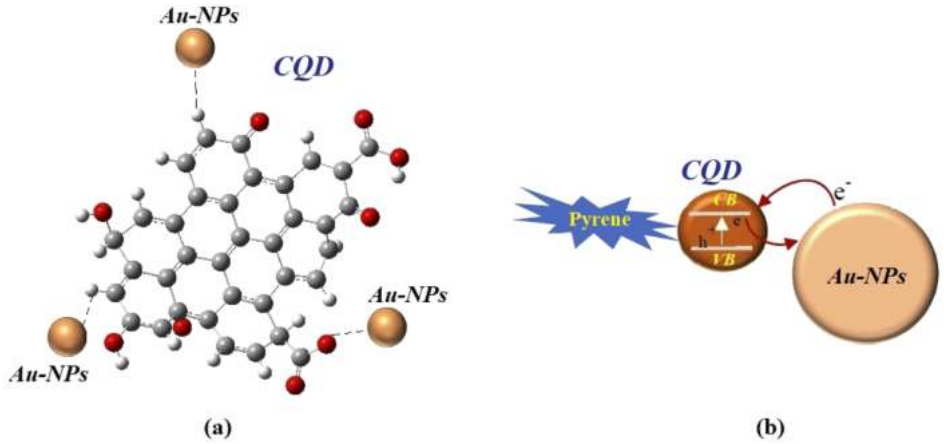

Fig. 8. a) The interaction model for capping the Au-NPs with CQD. b) The mechanism model for transfer electron between Au-NPs and CQD for the detection of pyrene.

4. Conclusion

The gold nanoparticles were fabricated in the CQD solution using the laser ablation technique to enhance the photoluminescence property of CQD. The ablation times were 4, 8, 12, and 16 mins. The particle size was investigated using TEM, which was in the range of 20.69 and 13.52 nm. The UV-Vis and FT-IR spectra confirmed that the Au-NPs were formed in the CQD, and TEM images authenticated that the nanoparticles were formed in the spherical shape. The results showed that when the ablation time increased, the particle size decreased. The plasmonic quality factor increased as the particle size increased. The photoluminescence spectra show that the excitation and the emission of Au-NPs/CQD solution occurred at 256 nm, and 336 nm, respectively, and the Au-NPs enhanced the photoluminescence property of CQD. The pure CQD

Optical Materials EXPRESS

and Au-NPs/CQD in the high concentration and lower particle size were used to detect the pyrene in the different concentration using photoluminescence spectroscopy. The results confirmed that when the Au-NPs/CQD interacted with pyrene, the variation of photoluminescence intensity peak was greater than the variation of the intensity peak in the presence of pure CQD. Therefore, Au-NPs not only enhanced the photoluminescence property of the CQD bath, but also improved the interaction of CQD with pyrene. The limit of the detection for pyrene was about 1 ppm in the presence of an Au-NPs/CQD composite. Consequently, CQD can be used when capping the Au-NPs and also it can interact with pyrene.

Acknowledgments

The authors acknowledge from Universiti Purta Malaysia and Institute of Advanced Technology (ITMA) UPM to provide the analytical facilities.

Disclosures

The authors declare no conflicts of interest.

References

1. M. J. Molaei, "A review on nanostructured carbon quantum dots and their applications in biotechnology, sensors, and chemiluminescence," Talanta **196**(1), 456–478 (2019).
2. S. Y. Lim, W. Shen, and Z. Gao, "Carbon quantum dots and their applications," Chem. Soc. Rev. **44**(1), 362–381 (2015).
3. S. Zhu, Q. Meng, L. Wang, J. Zhang, Y. Song, H. Jin, K. Zhang, H. Sun, H. Wang, and B. Yang, "Highly photoluminescent carbon dots for multicolor patterning, sensors, and bioimaging," Angew. Chem. **125**(14), 4045–4049 (2013).
4. N. Duran, M. B. Simões, A. de Moraes, W. J. Favaro, and A. B. Seabra, "Nanobiotechnology of carbon dots, a review," J. Biomed. Nanotechnol. **12**(7), 1323–1347 (2016).
5. F. Yuan, S. Li, Z. Fan, X. Meng, L. Fan, and S. Yang, "Shining carbon dots: synthesis and biomedical and optoelectronic applications," Nano Today **11**(5), 565–586 (2016).
6. X. Li, H. Wang, Y. Shimizu, A. Pyatenko, K. Kawaguchi, and N. Koshizaki, "Preparation of carbon quantum dots with tenable photoluminescence by rapid laser passivation in ordinary organic solvents," Chem. Commun. **47**(3), 932–934 (2011).
7. L. Cao, X. Wang, M. J. Meziani, F. Lu, H. Wang, P. G. Luo, Y. Lin, B. A. Harruff, L. M. Veca, and D. Murray, "Carbon dots for multiphoton bioimaging," J. Am. Chem. Soc. **129**(37), 11318–11319 (2007).
8. S. J. Phang and L.-L. Tan, "Recent advances in carbon quantum dot (CQD)-based two dimensional materials for photocatalytic applications," Catal. Sci. Technol. **9**(21), 5882–5905 (2019).
9. H. Li, X. He, Z. Kang, H. Huang, Y. Liu, J. Liu, S. Lian, C. H. A. Tsang, X. Yang, and S. T. Lee, "Water soluble fluorescent carbon quantum dots and photocatalyst design Angew," Angew. Chem., Int. Ed. **49**(26), 4430–4434 (2010).
10. Z. Ding, J. Wen, X. Wang, and R. Sun, "Gram-scale synthesis of single-crystalline graphene quantum dots derived from lignin biomas," Green Chem. **20**(6), 1383–1390 (2018).
11. Y. Liu, C. Liu, Zhang, and Zhi-Ying, "Synthesis and surface photochemistry of graphitized carbon quantum dots," J. Colloid Interface Sci. **356**(2), 416–421 (2011).
12. L. Brus, "Electronic wave functions in semiconductor clusters: experiment and theory," J. Phys. Chem. **90**(12), 2555–2560 (1986).
13. R. Ye, C. Xiang, J. Lin, Zh. Peng, K. Huang, Zh. Yan, N. P. Cook, E. L. G. Samuel, C. C. Hwang, G. Ruan, G. Ceriotti, A. R. O. Raji, A. A. Martí, M. Tour, and James, "Coal as an abundant source of graphene quantum dots," Nat. Commun. **4**(1), 2943 (2013).
14. S. Sarkar, D. Banerjee, U. K. Ghorai, N. S. Das, and K. K. Chattopadhyay, "Size dependent photoluminescence property of hydrothermally synthesized crystalline carbon quantum dots," J. Fluoresc. **178**, 314–323 (2016).
15. S. R. Zhang, Q. Wang, G. H. Tian, and H. G. Ge, "A fluorescent turn-off/on method for detection of Cu^{2+} and oxalate using carbon dots as fluorescent probes in aqueous solution," Mater. Lett. **115**, 233–236 (2014).
16. K. G. Qu, J. S. Wang, J. S. Ren, and X. G. Qu, "Carbon dots prepared by hydrothermal treatment of dopamine as an effective fluorescent sensing platform for the label-free detection of iron(III) ions and dopamine," Chem. - Eur. J. **19**(22), 7243–7249 (2013).
17. M. Zheng, Z. G. Xie, D. Qu, D. Li, P. Du, X. B. Jing, and Z. C. Sun, "On-off-on fluorescent carbon dot nanosensor for recognition of chromium(VI) and ascorbic acid based on the inner filter effect," ACS Appl. Mater. Interfaces **5**(24), 13242–13247 (2013).

Optical Materials EXPRESS

18. H. M. Goncalves, A. J. Duarte, and J. C. E. da Silva, "Optical fiber sensor for Hg(II) based on carbon dots," Biosens. Bioelectron. **26**(4), 1302–1306 (2010).
19. N. Elahi, M. Kamali, and M. H. Baghersad, "Recent biomedical applications of gold nanoparticles, A review," Talanta **184**, 537–556 (2018).
20. X. Zhang, "Gold nanoparticles: recent advances in the biomedical applications Cell," Cell Biochem. Biophys. **72**, 771–775 (2015).
21. M. A. K. Abdelhalim, M. M. Mady, and M. M. Ghannam, "Physical Properties of Different Gold Nanoparticles: Ultraviolet-Visible and Fluorescence Measurements," J. Nanomed. Nanotechnol. **3**(3), 1000133 (2012).
22. Y.-C. Yeh, B. Creran, and V. M. Rotello, "Gold nanoparticles: preparation, properties, and applications in bionanotechnology," Nanoscale **4**(6), 1871–1880 (2012).
23. X. Ye, Y. Gao, J. Chen, D. C. Reifsnyder, C. Zheng, and C. B. Murray, "Seeded growth of monodisperse gold nanorods using bromide-free surfactant mixtures," Nano Lett. **13**(5), 2163–2171 (2013).
24. F. Yuan, H. Chen, J. Xu, Y. Zhang, Y. Wu, L. Wang, and Aptamer, "based luminescence energy transfer from near_infrared_to_near_infrared upconverting nanoparticles to gold nanorods and its application for the detection of thrombin," Chem. - Eur. J. **20**(10), 2888–2894 (2014).
25. D. Yin, X. Li, Y. Ma, and Z. Liu, "Targeted cancer imaging and photothermal therapy via monosaccharideimprinted gold nanorods," Chem. Commun. **53**(50), 6716–6719 (2017).
26. M. Pita, M. Krämer, J. Zhou, A. Poghossian, M. J. Schöning, V. M. Fernández, and E. Katz, "Optoelectronic Properties of Nanostructured Ensembles Controlled by Biomolecular Logic Systems," ACS Nano **2**(10), 2160–2166 (2008).
27. R. S. Tomar and V. Shrivastava, "Synthesis of gold nanoparticles: a biological approach," International Journal of Multidisciplinary Educational Research. **3**, 119–137 (2014).
28. M. Soumya, S. Rajeshkumar, and S. Venkat Kumar, "A review on biogenic synthesis of gold nanoparticles, characterization, and its applications," Resour.-Effic. Technol. **3**(4), 516–527 (2017).
29. M. Shah, V. Badwaik, Y. Kherde, H. K. Waghwani, Z. P. T. Aguilar, H. Rodgers, W. Hamilton, T. Marutharaj, C. Webb, M. B. Lawrenz, and R. Dakshinamurthy, "Gold nanoparticles: various methods of synthesis and antibacterial applications," Front. Biosci., Landmark Ed. **19**(8), 1320–1344 (2014).
30. R. Das, P. J. Babu, N. Gogoi, P. Sharma, and U. Bora, "Microwave-mediated rapid synthesis of gold nanoparticles Using Calotropis procera latex and study of optical properties," ISRN Nanomaterials 2012, ID650759 (2012).
31. K. Okitsu, M. Ashokkumar, and F. Grieser, "Sonochemical synthesis of gold nanoparticles: effects of ultrasound frequency," J. Phys. Chem. B **109**(44), 20673–20675 (2005).
32. P. H. N. Diem, D. T. T. Thao, D. V. Phu, N. N. Duy, H. T. D. Quy, T. T. Hoa, and N. Q. Hien, "Synthesis of Gold Nanoparticles Stabilized in Dextran Solution by Gamma Co-60 Ray Irradiation and Preparation of Gold Nanoparticles/Dextran Powder," J. Chem. **2017**, 1–8 (2017).
33. Y. Shi, Y. Pan, H. Zhang, Z. Zhang, M.-J. Li, C. Yi, and M. A. Yang, "A dual-mode nanosensor based on carbon quantum dots and gold nanoparticles for discriminative detection of glutathione in human plasma," Biosens. Bioelectron. **56**, 39–45 (2014).
34. B. Bagra, W. Zhang, Z. Zeng, T. Mabe, and J. Wei, "Plasmon-Enhanced Fluorescence of Carbon Nanodots in Gold Nanoslit Cavities," Langmuir **35**(27), 8903–8909 (2019).
35. D. Yoo, Y. Park, B. Cheon, and M. H. Park, "Carbon Dots as an Effective Fluorescent Sensing Platform for Metal Ion Detection," Nanoscale Res. Lett. **14**(1), 272–285 (2019).
36. J. Korram, L. Dewangan, R. Nagwanshi, I. Karbhal, K. K. Ghosh, and M. L. Satnami, "A carbon quantum dot–gold nanoparticle system as a probe for the inhibition and reactivation of acetylcholinesterase detection of pesticides," New J. Chem. **43**(18), 6874–6882 (2019).
37. A. M. R. Shokri and T. Hallaj, "Interaction of glucose-derived carbon quantum dots with silver and gold nanoparticles and its application for the fluorescence detection of 6-thioguanine," Luminescence **32**(3), 292–297 (2017).
38. J. Song, L. Zhao, Y. Wang, Y. Xue, Y. Deng, X. Zhao, and Q. Li, "Carbon Quantum Dots Prepared with Chitosan for Synthesis of CQDs/AuNPs for Iodine Ions Detection," Nanomaterials **8**(12), 1043 (2018).
39. A. Mehta and A. Mishra, "Optical Detection of Thiol Drugs by Core–Shell Luminous Carbon Dots—Gold Nanoparticles System," Plasmonics **13**(6), 2239–2248 (2018).
40. Z. C. Zhang, Q. L. Ma, and J. L. Li, "Preparation of gold nanoparticles and carbon dots by hydrothermal reaction of bovine haemoglobin with chloroauric acid and energy band bending in carbon dots," J. Exp. Nanosci. **12**(1), 239–246 (2017).
41. R. Changerath, S. Kunnatheery, and R. Joseph, "Physical Mixture of Gold Nanoparticles and Carbon Dots Enable Sensing of Cyanide Ions in Water in Dual Modes," Nano. Res. Appl. **5**, 40 (2019).
42. M. Kim, S. Osone, T. Kim, H. Higashi, and T. Seto, "Synthesis of Nanoparticles by Laser Ablation: A Review," KONA **34**(0), 80–90 (2017).
43. A. R. Sadrolhosseini, S. A. Rashid, and A. Zakaria, "Synthesis of gold nanoparticles dispersed in palm oil using laser ablation technique," J. Nanomater. **2017**, 6496390 (2017).
44. X. Ren, F. Zhang, B. Guo, N. Gao, and X. Zhang, "Synthesis of N-Doped Micropore Carbon Quantum Dots with High Quantum Yield and Dual-Wavelength Photoluminescence Emission from Biomass for Cellular Imaging," Nanomaterials **9**(4), 495 (2019).

Optical Materials EXPRESS

45. D. Reyes, M. Camacho, M. Camacho, M. Mayorga, D. Weathers, G. Salamo, Z. Wang, and A. Neogi, "Laser Ablated Carbon Nanodots for Light Emission," Nanoscale Res. Lett. **11**(1), 424 (2016).
46. M. J. Molaei, "Carbon quantum dots and their biomedical and therapeutic applications: a review," RSC Adv. **9**(12), 6460–6481 (2019).
47. H. Abdelsalam, H. Elhaes, and M. A. Ibrahim, "Tuning electronic properties in graphene quantum dots by chemical functionalization: Density functional theory calculations," Chem. Phys. Lett. **695**(2018), 138–148 (2018).
48. J. Feng, H. Dong, L. Yu, and L. Dong, "The optical and electronic properties of graphene quantum dots with oxygen-containing groups: a density functional theory study," J. Mater. Chem. C **5**(24), 5984–5993 (2017).
49. A. R. Sadrolhosseini, S. A. Rashid, S. Shafie, and H. Soleimani, "Laser ablation synthesis of Ag nanoparticles in graphene quantum dots aqueous solution and optical properties of nanocomposite," Appl. Phys. A **125**, 82 (2019).
50. R. S. da Costa, W. F. da Cunha, N. S. Pereira, and A. M. Ceschin, "An Alternative Route to Obtain Carbon Quantum Dots from Photoluminescent Materials in Peat," *Materials* 11(2018) 1492.
51. S. Ge, M. Yan, J. Lu, J. Lua, M. Zhanga, F. Yub, J. Yu, X. Songc, and S. Yu, "Electrochemical biosensor based on graphene oxide–Au nanoclusters composites for l-cysteine analysis," Biosens. Bioelectron. **31**(1), 49–54 (2012).
52. A. R. Sadrolhosseini, S. A. Rashid, N. Jamaludin, and A. M. Isloor, "Experimental and molecular modeling of interaction of carbon quantum dots with glucose," Appl. Phys. A **125**(8), 529 (2019).
53. P. Shemella, Y. Zhang, and M. Mailman, "Energy gaps in zero-dimensional graphene nanoribbons," Appl. Phys. Lett. **91**(4), 042101 (2007).
54. C. M. Carbonaro, R. Corpino, M. Salis, F. Mocci, S. V. Thakkar, C. Olla, and P. C. Ricci, "On the Emission Properties of Carbon Dots: Reviewing Data and Discussing Models," C **5**(4), 60–75 (2019).
55. Y. Tang, X. Yu, J. Xu, B. Audit, and S. Zhang, "Applications of Hybrid Nanoparticles in Biosensors: Simulation Studies, Noble Metal-Metal Oxide Hybrid Nanoparticles, Fundamentals and Applications," *Micro and Nano Technologies*, 431–455 (2019).
56. R. Tsekov, P. Georgiev, S. Simeonova, and K. Balashev, "Quantifying the Blue Shift in the Light Absorption of Small Gold Nanoparticles," C. R. Acad. Bulg. Sci. **70**, 1237–1246 (2017).
57. P. Mulvaney, "Surface plasmon spectroscopy of nanosized metal particles," Langmuir **12**(3), 788–800 (1996).
58. P. Georgiev, A. Bojinova, B. Kostova, D. Momekova, T. Bjornholm, and K. Balashev, "Implementing atomic force microscopy (AFM) for studying kinetics of gold nanoparticle's growth," Colloids Surf., A **434**, 154–163 (2013).
59. P. Georgiev, S. Simeonova, A. Chanachev, L. Michaylov, D. Nihtianova, and K. Balashev, "Acceleration effect of copper(II) ions on the rate of citrate synthesis of gold nanoparticles," Colloids Surf., A **494**, 39–48 (2016).
60. A. R. Sadrolhosseini, S. A. Rashid, S. Shafie, and H. Nezakati, "Laser ablation synthesis of gold nanoparticle to enhance the fluorescence properties of graphene quantum dots," J. Laser Appl. **31**(2), 022006 (2019).
61. A. T. R. Williams, S. A. Winfield, and J. N. Miller, "Relative Fluorescence Quantum Yields Using a Computer controlled Luminescence Spectrometer," Analyst **108**(1290), 1067–1071 (1983).
62. R. Gui, X. Liu, H. Jin, Z. Wang, F. Zhang, J. Xia, M. Yang, S. Bi, and Y. Xia, "Retracted: N, S co-doped graphene quantum dots from a single source precursor used for photodynamic cancer therapy under two-photon excitation," Chem. Commun. **51**(49), 10066 (2015).
63. A. Dager, T. Uchida, T. Maekawa, and M. Tachibana, "Synthesis and characterization of Mono-disperse Carbon Quantum Dots from Fennel Seeds: Photoluminescence analysis using Machine Learning," Sci. Rep. **9**(1), 14004 (2019).
64. X. Liu, X. J. Pang, F. Xu, and X. Zhang, "Simple Approach to Synthesize Amino-Functionalized Carbon Dots by Carbonization of Chitosan," Sci. Rep. **6**(1), 31100 (2016).
65. Y. Dong, "Natural carbon-based dots from humic substances," Sci. Rep. **5**(1), 10037 (2015).
66. Z. Gan, H. Xu, and Y. Hao, "Mechanism for excitation-dependent photoluminescence from graphene quantum dots and other graphene oxide derivates: consensus, debates and challenges," Nanoscale **8**(15), 7794–7807 (2016).
67. L. Cao, M. J. Meziani, S. Sahu, and Y. P. Sun, "Photoluminescence properties of graphene versus other carbon nanomaterials," Acc. Chem. Res. **46**(1), 171–180 (2013).
68. P. Demchenko and M. O. Dekaliuk, "Novel fluorescent carbonic nanomaterials for sensing and Imaging," Methods Appl. Fluoresc. **1**(4), 042001 (2013).
69. Q. Xu, T. Kuang, Y. Liu, L. Cai, X. Peng, T. S. Sreeprasad, P. Zhao, Z. Yu, and N. Li, "Heteroatomdoped carbon dots: Synthesis, characterization, properties, photoluminescence mechanism and biological applications," J. Mater. Chem. B. **4**(45), 7204–7219 (2016).